IEEE Access
Multidisciplinary | Rapid Review | Open Access Journal

Received August 30, 2017, accepted September 28, 2017, date of publication October 11, 2017,
date of current version November 7, 2017.

Digital Object Identifier 10.1109/ACCESS.2017.2762240

Performance Analysis of Distributed Auxiliary Radio Telescopes Under Shared Spectrum Access Paradigm and Cooling Power Constraint

DONG HAN, (Student Member, IEEE), AND HLAING MINN, (Fellow, IEEE)
Department of Electrical and Computer Engineering, The University of Texas at Dallas, Richardson, TX 75080, USA

Corresponding author: Hlaing Minn (hlaing.minn@utdallas.edu)

This work was supported by the National Science Foundation under Grant 1547048.

ABSTRACT A conflict of the spectrum rights and needs between active wireless communication systems and passive radio astronomy systems (RASs) has become substantially greater due to the phenomenal expansion of wireless communications and increased interest in RAS observation. For sustainable growth and coexistence of cellular wireless communications (CWC) and RAS, a coordinated shared spectrum access paradigm was recently introduced. Embracing such paradigm, this paper proposes a distributed auxiliary radio telescope (DART) system which can geographically and spectrally coexist with CWC while offering additional capability or performance enhancement to RAS. Theoretical performance analysis of the DART system with different quantization resolutions is presented, and approximate closed-form expressions are obtained. Adaptation of cooling power of DART receivers according to the time-varying ambient temperature is also proposed. Furthermore, an analytical expression for the DART system parameters under the shared spectrum access paradigm and cooling power constraint to achieve the same performance as the existing single-dish RAS with a radio quiet zone is developed to provide guidance in the DART system design. The numerical and simulation results illustrate feasibility and potentials of the proposed DART system.

INDEX TERMS Spectrum sharing, ADC resolution, distributed auxiliary radio telescopes, noise referencing, cooling power allocation.

I. INTRODUCTION

RAS provides economically and scientifically important observations of the cosmos which benefit the society consistently [2]. As RAS signals are very weak with signal-to-noise power ratio (SNR) as low as −60 dB [3], they are highly sensitive to radio frequency interference (RFI) caused by wireless communication systems. Thus, radio telescopes are built in remote areas surrounded by radio quiet zones for interference isolation [4], [5]. However, the expansion of wireless communication systems in terms of applications [6], radio coverage, radio spectrum [7], and spectrum utilization [8]–[10] has caused increased RFI to RAS. The direct results are RFI-corrupted radio astronomical data and less radio astronomical observation opportunities and the consequence is a severe hindrance to science and knowledge discovery.[1] On the other hand, there are increased interests and needs for expanding RAS observations, thus enlarging the conflict of spectrum access rights/needs between the two systems [11]–[13].

There are two types of RAS, namely single-dish telescope and telescope array. Single-dish telescope has unique advantages such as good potential sensitivity to large scale structure, building and maintaining simplicity and upgrading flexibility [14]. Numerous single-dish telescopes have been built, e.g., the 305-meter Arecibo Observatory built in 1963 and the Five hundred meter Aperture Spherical Telescope (FAST) completed in last year. Nevertheless, the single-dish telescope also has shortcomings in spatial frequency response and mechanical complexity perspectives [14] compared with the radio telescope array. Processing the signals received by a telescope array can mitigate the interference and increase the observation range and resolution. Therefore, we have also seen the prosperity of radio telescope arrays such as the Very Large Array (VLA) and the Square Kilometer Array (SKA) and a trend of combination among single-dish telescopes and telescope arrays. Nevertheless, these existing RAS sites are protected by radio quiet zones and cannot coexist with CWC.

[1]The CWC systems from the second generation to the fourth generation use the frequency bands from 450 MHz to 2.6 GHz. The fifth generation CWC systems are expected to use additional higher frequency bands up to the millimeter-wave band. However, RAS interested bands cover an even wider spectrum range, from several MHz to hundreds of GHz, including the whole spectrum bands allocated to current and future wireless communications.

To mitigate the conflict between CWC and RAS, [15] and [16] recently proposed a new spectrum sharing paradigm where both systems have RFI-free guaranteed spectrum access by means of a three-phase time-division approach. Differences between such paradigm and the cognitive radio spectrum sharing approaches are also described in [16]. It pointed out the instancy of embracing the new paradigm and justified that different from other spectrum sharing schemes [17]–[22] for cognitive radio, the overall spectrum utilization is enhanced by designing time-dependent durations of the spectrum access phases according to the CWC traffic statistics (e.g., on an hourly basis). An extension for coexistence of WiFi and RAS was addressed in [23].

Technical Contributions: To accommodate expansions of both CWC and RAS, we embrace the shared spectrum access paradigm of [15] and propose a DART system which can coexist with CWC and conventional single-dish RAS. Our DART system can either work independently as a radio telescope array or cooperate with an existing single-dish RAS to increase the overall performance accuracy. We derive analytical performance expressions for signal power estimation of the DART system with different quantization resolutions, and then obtain approximate closed-form expressions. We observe that a larger resolution of analog-to-digital converter (ADC) yields a smaller bias but a larger variance to the RAS signal power estimation. These biases remain relatively constant within the typical range of RAS signal-to-noise ratio (SNR), thus the bias can be compensated. However, after the bias compensation, the resulting variance of the RAS signal power estimate is also changed and a higher ADC resolution provides better performance in terms of estimation variance (after the bias compensation). Next, we also obtain an analytical expression for the DART system parameters under the shared spectrum access paradigm to achieve the same performance as the existing single-dish RAS with a radio quiet zone. This provides guidance in the DART system design. These contributions are reported in our conference paper [1]. Additional contributions with respect to [1] are described below. We develop efficient combination of astronomical source power estimations between the single dish RAS and the DART system. Furthermore, cooling is a major source of operation cost for RAS. Given finite cooling power, we propose a dynamic cooling temperature approach to allocate the cooling power according to ambient temperatures and CWC traffic statistics. We investigate both perfect and imperfect temperature information scenarios for the cooling power allocation problem and a neat solution is found by using an alternating optimization approach. The numerical and simulation results illustrate performance of the proposed DART system as well as effects of ADC resolution on the RAS signal power estimation performance.

This paper is organized as follows. Section II introduces the RAS signal power estimation method and the system structure for both single-dish RAS and the DART system. We investigate the performance statistics of the astronomical signal power estimation under various ADC resolutions in Section III. Then in Section IV, we provide their closed-form approximations and investigate their relationships to the accurate (non-closed-form) expressions derived in the previous section. Next, Section V presents performance of the DART system under the three-phase spectrum sharing paradigm of [15] with reference to that of the single-dish RAS in a radio quiet zone. In Section VI, the cooling power allocation problem is proposed and investigated. Finally, Section VII concludes this paper.

II. SYSTEM MODEL

To enable growth in both CWC and RAS services, we consider the shared spectrum access paradigm proposed in [15] where CWC and RAS can coexist geographically and spectrally. Such coexistence paradigm removes the need of a radio quiet zone around each radio telescope and hence we propose to exploit it by introducing several radio telescopes within the radio coverage zones of CWC, which we term distributed auxiliary radio telescopes (DARTs). An illustration of the proposed system is shown in Fig. 1. The RAS data from each DART are saved at a central station or a cloud database center and hence cross-processing of data from different DARTs can be easily done. This coexistence paradigm could also promote emergence of DARTs set up by public institutions, private groups or individuals with strong interest in RAS.

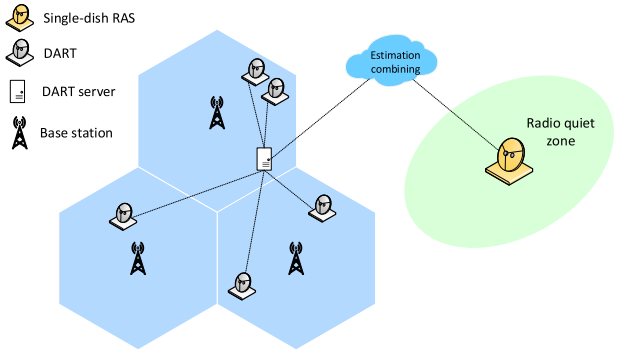

FIGURE 1. Geometric structure of the DART system and the single-dish RAS.

In the shared spectrum access approach of [15], a time frame of duration τ_{f}, which consists of n_{f} subframes of duration τ_{sf} each, is divided into three phases, namely CWC only phase of duration τ_{CWC} (n_{CWC} subframes), CWC+RAS phase of duration $\tau_{\mathrm{CWC+RAS}}$ ($n_{\mathrm{CWC+RAS}}$ subframes) and RAS only phase of duration τ_{RAS} (n_{RAS} subframes), as is shown in Fig. 2. The first phase is only for CWC while the last phase is only for RAS, thus providing RFI-free spectrum access to both systems. The second phase is used to absorb different propagation delays of CWC cells, and it could allow transmissions in some CWC cells, some practical testing of RFI cancellation schemes, or fine tuning of the shared spectral access paradigm [16]. The durations of the three phases can be adjusted based on the spectrum access needs, the CWC traffic statistics, and practical fine tuning results of

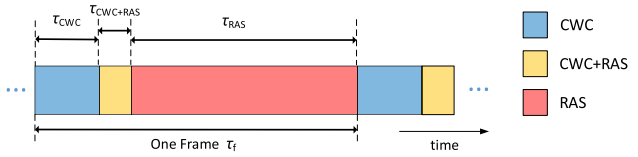

FIGURE 2. Frame structure of the three-phase spectrum sharing paradigm where the durations of the phases could be different at different hours [15].,

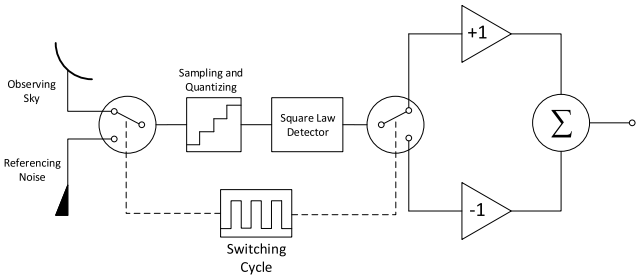

FIGURE 3. RAS receiver structure with noise referencing.

the shared spectrum access parameters. An example of spectrum access duration adaptation on an hourly basis[2] based on the CWC traffic statistics was presented in [15]. For our DART deployment, to guarantee RFI-free observation, we only use the RAS only phase for the DART. The implication of this shared spectrum access is the reduction of the RAS observation time of a DART if compared to the RAS in a radio quiet zone. However, more DARTs can be used to recover the loss in the RAS observation time or to get even a larger effective observation time. In the following, we will develop signal model, estimator, and performance analysis in a general sense based on the number of observation samples and the noise variance. By substituting appropriate values for those parameters, one can obtain the results for the the considered scenario or paradigm.

The DART system aims to receive the radio waves of the astronomical radio sources, which are commonly modeled to be zero mean complex Gaussian distributed [24]–[27], and then estimate the power of the source in terms of the radiation power. However, the received radio wave sent from the source is significantly weaker than the additive thermal noise at the receiver. To mitigate the noise impact and achieve unbiased power estimation as accurate as possible, we apply a noise referring approach called Dicke switching (see [28, Fig. 4.8] and [29]) where the receivers switch the observations between astronomical source and the inner noise generating source.[3] The simplified receiver structure is shown in Fig. 3. Each antenna element samples and quantizes the astronomical radio signal corrupted with additive thermal noise and the reference thermal noise in a time-division manner. Next, the quantized samples are squared by the detector to obtain the signal power. Subtracting the averaged reference samples' power from the averaged noise corrupted astronomical samples' power, the power of astronomical radio signal is estimated. To be specific, for the DART system with M antenna elements (telescopes), we assume the received astronomical source signal at each antenna is circular symmetric complex Gaussian (CSCG) distributed with zero mean and variance σ_s^2. We also assume the additive thermal noise at each antenna is distributed as zero mean CSCG with the same variance σ_n^2. Therefore, the nth samples of the received astronomical source signal, the noise involved in astronomical observation and the referencing noise at the ith antenna are represented as $s_t^i(n)$, $n_t^i(n)$ and $n_r^i(n)$, respectively, where $i \in \{1, ..., M\}$. We assume that the received signals are independent over different samples. Besides, the quantization errors of the nth sample at the ith antenna are $e_t^i(n)$ and $e_r^i(n)$ for astronomical observation and noise referencing, respectively. Correspondingly, the quantized samples are represented as

$$y_t^i(n) \triangleq s_t^i(n) + n_t^i(n) + e_t^i(n) \tag{1}$$

$$y_r^i(n) \triangleq n_r^i(n) + e_r^i(n) \tag{2}$$

where $s_t^i(n) \sim CN(0, \sigma_s^2)$ and $n_t^i(n), n_r^i(n) \sim CN(0, \sigma_n^2)$. Assuming we have a fixed observation time with a fixed sampling frequency, which corresponds to $2L$ samples, it can be shown that the most accurate power estimation is achieved asymptotically if we allocate L samples for astronomical observation and L samples for referencing when the following two criteria are satisfied, 1) negligible quantization error and 2) $\frac{\sigma_s^2}{\sigma_n^2} \to 0$. The proof is provided in Section IV. By applying this result, the output estimated source power is

$$\rho_{\text{array}} = \frac{1}{ML} \sum_{i=1}^{M} \sum_{n=1}^{L} \left\{ |y_t^i(n)|^2 - |y_r^i(n)|^2 \right\}. \tag{3}$$

Since there is only one antenna element in the single-dish system, it can be regarded as a special case of the array system. Assuming we have in total $2N$ samples and allocate N samples for astronomical observation and another N samples for noise referencing, the output estimated source power is

$$\rho_{\text{single}} = \frac{1}{N} \sum_{n=1}^{N} \left\{ |y_t(n)|^2 - |y_r(n)|^2 \right\} \tag{4}$$

where $y_t(n)$ and $y_r(n)$ represent the quantized samples for astronomical observation and noise referencing of single-dish RAS, respectively.

Suppose the hourly based resource adaptation of [15] is applied and the three phases (see Fig. 2) at hour l have per-frame durations $\tau_{\text{CWC},l}$ ($n_{\text{CWC},l}$ subframes), $\tau_{\text{CWC+RAS},l}$ ($n_{\text{CWC+RAS},l}$ subframes) and $\tau_{\text{RAS},l}$ ($n_{\text{RAS},l}$ subframes), respectively, and $\tau_{\text{CWC},l} + \tau_{\text{CWC+RAS},l} + \tau_{\text{RAS},l} = \tau_f$. The total number of frames per hour is $N_{\text{f/hour}} = 3600/\tau_f$. Suppose the sampling frequency is $2B$ for RAS and the RAS signal power estimation is done based on K hours $\{l_k : k = 1, \cdots, K\}$. Then the number of samples available for a single DART is $2L = 2B \sum_{k=1}^{K} \tau_{\text{RAS},l_k} N_{\text{f/hour}}$ while that for the conventional single-dish RAS, since the

[2]computed and designed in advance, thus no online adaptation is needed.
[3]Other noise referencing approaches can also be applied.

spectrum is not shared, is $2N = 2BK\tau_{\rm f}N_{\rm f/hour}$. Obviously, as $\sum_{k=1}^{K}\tau_{{\rm RAS},l_k} < K\tau_{\rm f}$, the RAS observation time for DARTs is smaller than that for the single-dish RAS with radio quiet zones. However, under the spectrum sharing paradigm, several (M) telescopes can coexist with CWC and the total number of samples available is increased by M as can be seen in (3) for the DART system.

III. PERFORMANCE ANALYSIS OF RAS SIGNAL POWER ESTIMATION UNDER FINITE ADC RESOLUTIONS

In this section, we analyze the mean and variance of the estimated astronomical source power for both systems. We mainly focus on the DART system since the results are naturally applicable to the single-dish RAS by setting $M = 1$. Since the in-phase component and the quadrature-phase component of the signals are independently and identically distributed (i.i.d.), we represent the estimated power $\rho_{\rm array}$ as the sum of two i.i.d. parts, namely the in-phase estimated power $\rho_{\rm in}$ and the quadrature-phase estimated power $\rho_{\rm quad}$, i.e., $\rho_{\rm array} = \rho_{\rm in} + \rho_{\rm quad}$ where

$$\rho_{\rm in} = \frac{1}{ML}\sum_{i=1}^{M}\sum_{n=1}^{L}\left(\Re\{y_{\rm t}^{i}(n)\}^2 - \Re\{y_{\rm r}^{i}(n)\}^2\right) \quad (5)$$

$$\rho_{\rm quad} = \frac{1}{ML}\sum_{i=1}^{M}\sum_{n=1}^{L}\left(\Im\{y_{\rm t}^{i}(n)\}^2 - \Im\{y_{\rm r}^{i}(n)\}^2\right). \quad (6)$$

Given a b-bit quantizer with the quantization thresholds and quantized values being represented as v_k, $k \in \{1,\ldots,2^b+1\}$, and c_k, $k \in \{1,\ldots,2^b\}$, respectively, the second moment of the real-part quantized sample is

$$\begin{aligned}\mathbb{E}\left[\Re\{y_{\rm p}^{i}(n)\}^2\right] &= \sum_{k=1}^{2^b}\int_{v_k}^{v_{k+1}} c_k^2 f_{\rm p}(x)dx \\ &= \sum_{k=1}^{2^b} c_k^2\left[Q(v_k/\sigma_{\rm p}) - Q(v_{k+1}/\sigma_{\rm p})\right] \quad (7)\end{aligned}$$

where ${\rm p} \in \{{\rm t},{\rm r}\}$, $\sigma_{\rm t}^2 = \frac{\sigma_{\rm s}^2+\sigma_{\rm n}^2}{2}$, $\sigma_{\rm r}^2 = \frac{\sigma_{\rm n}^2}{2}$, $f_{\rm p}(x)$ is the Gaussian probability density function with zero mean and variance $\sigma_{\rm p}^2$, and $Q(x) = \frac{1}{\sqrt{2\pi}}\int_x^\infty e^{-u^2/2}du$. And we have $\mathbb{E}\left[\Re\{y_{\rm p}^{i}(n)\}^2\right] = \mathbb{E}\left[\Im\{y_{\rm p}^{i}(n)\}^2\right]$. Define

$$\varphi_{\rm p} \triangleq \sum_{k=1}^{2^b} c_k^2\left[Q(v_k/\sigma_{\rm p}) - Q(v_{k+1}/\sigma_{\rm p})\right], \quad {\rm p}\in\{{\rm t},{\rm r}\} \quad (8)$$

$$\phi_{\rm p} \triangleq \sum_{k=1}^{2^b} c_k^4\left[Q(v_k/\sigma_{\rm p}) - Q(v_{k+1}/\sigma_{\rm p})\right], \quad {\rm p}\in\{{\rm t},{\rm r}\}. \quad (9)$$

Then, from (5)-(7), we can represent the first moment of the in-phase and quadrature-phase estimated powers as

$$\mathbb{E}[\rho_{\rm in}] = \mathbb{E}[\rho_{\rm quad}] = \varphi_{\rm t} - \varphi_{\rm r}. \quad (10)$$

We can also obtain their second moments $\mathbb{E}\left[\rho_{\rm in}^2\right] = \mathbb{E}\left[\rho_{\rm quad}^2\right]$ as in (11) shown at the bottom of the next page, where the approximation (a) is due to the independence assumption between $y_{\rm t}^{i}(n)$ and $y_{\rm t}^{j}(n)$, $\forall i \neq j$. As the power of astronomical source is significantly less than the power of noise, the approximated expression in (11) is asymptotically accurate when the received SNR approaches zero. According to (10) and (11), the variance of the in-phase estimated power and that of the quadrature-phase estimate power are

$$\mathrm{Var}(\rho_{\rm in}) = \mathrm{Var}(\rho_{\rm quad}) \approx \frac{1}{ML}(\phi_{\rm t}+\phi_{\rm r}-\varphi_{\rm t}^2-\varphi_{\rm r}^2). \quad (12)$$

Then, we obtain the mean and variance of the power estimation of the DART system as

$$\mathbb{E}[\rho_{\rm array}] = \mathbb{E}[\rho_{\rm in}] + \mathbb{E}[\rho_{\rm quad}] = 2(\varphi_{\rm t}-\varphi_{\rm r}) \quad (13)$$

$$\begin{aligned}\mathrm{Var}(\rho_{\rm array}) &= \mathrm{Var}(\rho_{\rm in}) + \mathrm{Var}(\rho_{\rm quad}) \\ &\approx \frac{2}{ML}(\phi_{\rm t}+\phi_{\rm r}-\varphi_{\rm t}^2-\varphi_{\rm r}^2). \quad (14)\end{aligned}$$

Next, by seting $M = 1$ and substituting L with N, we also obtain the counterparts for the single-dish RAS as

$$\mathbb{E}[\rho_{\rm single}] = 2(\varphi_{\rm t}-\varphi_{\rm r}) \quad (15)$$

$$\mathrm{Var}(\rho_{\rm single}) = \frac{2}{N}(\phi_{\rm t}+\phi_{\rm r}-\varphi_{\rm t}^2-\varphi_{\rm r}^2). \quad (16)$$

Note that (16) is an accurate expression since for $M = 1$, (11) involves no approximation. Besides, as the effect of the noise variance is embedded in $\varphi_{\rm t}$, $\varphi_{\rm r}$, $\phi_{\rm t}$, and $\phi_{\rm r}$, a different noise variance could affect the mean and variance of the RAS power estimate. We also notice that for both the DART system and the single-dish RAS, the mean values of the output power estimates are the same as long as they have identical quantizer settings and the same noise variance. However, the variances of the output power estimates have different factors ML versus N. This clearly shows that although $L < N$, the DART system can improve its performance by increasing the number of antennas, M.

IV. APPROXIMATE CLOSED-FORM ANALYSIS

The means and variances of the estimated powers derived in (13) - (16) are not in closed forms. To have better insights, in this section, we develop approximated closed-form representations, assuming the received sample is independent from the quantization error.

For the DART system, conditioning on the quantization errors, the received signals are regarded as being i.i.d. CSCG distributed over all the antennas, i.e.,

$$\begin{aligned}y_{\rm t}^{i}(n)|e_{\rm t}^{i}(n) &\sim CN(e_{\rm t}^{i}(n), \sigma_{\rm n}^2+\sigma_{\rm s}^2) \\ y_{\rm r}^{i}(n)|e_{\rm r}^{i}(n) &\sim CN(e_{\rm r}^{i}(n), \sigma_{\rm n}^2). \quad (17)\end{aligned}$$

To prove the asymptotically optimal sample partitioning mentioned in Section II, we start the analysis by using different numbers of samples for source observation and noise referencing, namely, L_1 and L_2. Then, the estimated source power is rewritten as

$$\rho_{\rm array} = \frac{1}{ML_1}\sum_{i=1}^{M}\sum_{n=1}^{L_1}|y_{\rm t}^{i}(n)|^2 - \frac{1}{ML_2}\sum_{i=1}^{M}\sum_{n=1}^{L_2}|y_{\rm r}^{i}(n)|^2 \quad (18)$$

where $L_1 + L_2 = 2L$. For compactness, we define conditional terms $Z_{\rm t}^i \triangleq \sum_{n=1}^{L_1} |y_{\rm t}^i(n)|e_{\rm t}^i(n)|^2$ and $Z_{\rm r}^i \triangleq \sum_{n=1}^{L_2} |y_{\rm r}^i(n)|e_{\rm r}^i(n)|^2$ and note that both terms, $Z_{\rm t}^i$ and $Z_{\rm r}^i$, are non-central chi-square random variables with the means and variances being represented as

$$\mathbb{E}(Z_{\rm t}^i) = L_1(\sigma_{\rm n}^2 + \sigma_{\rm s}^2) + \sum_{n=1}^{L_1} |e_{\rm t}^i(n)|^2 \tag{19}$$

$$\mathbb{E}(Z_{\rm r}^i) = L_2\sigma_{\rm n}^2 + \sum_{n=1}^{L_2} |e_{\rm r}^i(n)|^2 \tag{20}$$

$$\mathrm{Var}(Z_{\rm t}^i) = L_1(\sigma_{\rm n}^2 + \sigma_{\rm s}^2)^2 + 2(\sigma_{\rm n}^2 + \sigma_{\rm s}^2)\sum_{n=1}^{L_1} |e_{\rm t}^i(n)|^2 \tag{21}$$

$$\mathrm{Var}(Z_{\rm r}^i) = L_2\sigma_{\rm n}^4 + 2\sigma_{\rm n}^2\sum_{n=1}^{L_2} |e_{\rm r}^i(n)|^2. \tag{22}$$

Therefore, conditioning on the quantization error set $\mathcal{E} = \{(e_{\rm t}^i(n), e_{\rm r}^i(m)) : i = 1, ..., M,\ n = 1, ..., L_1,\ m = 1, ..., L_2\}$, the estimated power is

$$\rho_{\rm array}|\mathcal{E} = \frac{1}{ML_1}\sum_{i=1}^{M} Z_{\rm t}^i - \frac{1}{ML_2}\sum_{i=1}^{M} Z_{\rm r}^i. \tag{23}$$

From (19) to (22), the mean and variance of $\rho_{\rm array}|\mathcal{E}$ are

$$\mu_{\rho|\mathcal{E}} = \mathbb{E}[\rho_{\rm array}|\mathcal{E}] = \sigma_{\rm s}^2 + \frac{\mathrm{MSE_t}(L_1)}{ML_1} - \frac{\mathrm{MSE_r}(L_2)}{ML_2} \tag{24}$$

$$\mathrm{Var}(\rho_{\rm array}|\mathcal{E}) = \frac{1}{ML_1}(\sigma_{\rm n}^2 + \sigma_{\rm s}^2)^2 + \frac{1}{ML_2}\sigma_{\rm n}^4 + \frac{2(\sigma_{\rm n}^2 + \sigma_{\rm s}^2)}{M^2L_1^2}\mathrm{MSE_t}(L_1) + \frac{2\sigma_{\rm n}^2}{M^2L_2^2}\mathrm{MSE_r}(L_2) \tag{25}$$

where $\mathrm{MSE_p}(L) \triangleq \sum_{i=1}^{M}\sum_{n=1}^{L} |e_{\rm p}^i(n)|^2,\ {\rm p} \in \{{\rm t}, {\rm r}\}$.

Now, we are able to find the asymptotically optimal sample numbers L_1 and L_2 based on the conditional variance in (25). Under the condition that the quantization error is negligible and $\frac{\sigma_{\rm s}^2}{\sigma_{\rm n}^2} \to 0$, we have

$$\lim_{e_{\rm t}^i, e_{\rm r}^i, \frac{\sigma_{\rm s}^2}{\sigma_{\rm n}^2}\to 0} \mathrm{Var}(\rho_{\rm array}) = \lim_{e_{\rm t}^i, e_{\rm r}^i, \frac{\sigma_{\rm s}^2}{\sigma_{\rm n}^2}\to 0} \mathrm{Var}(\rho_{\rm array}|\mathcal{E}) = \frac{\sigma_{\rm n}^4}{ML_1} + \frac{\sigma_{\rm n}^4}{ML_2}. \tag{26}$$

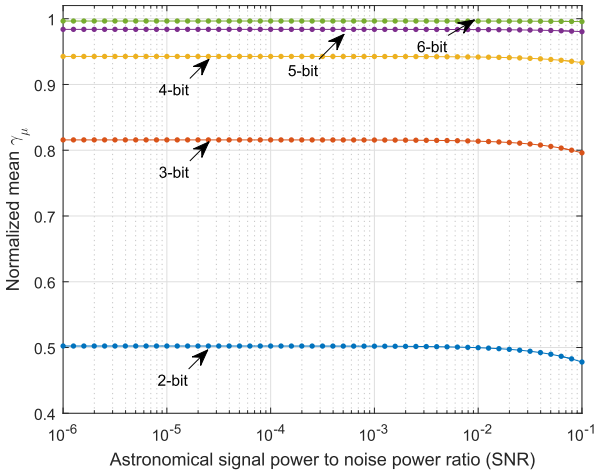

FIGURE 4. The normalized mean of RAS signal power estimation under various ADC resolutions ($\sigma_s^2 = 1$, N or $L = 10^4$).

With the fact that $L_1 + L_2 = 2L$, the minimum variance, i.e., the minimum of (26), is achieved when

$$L_1 = L_2 = L. \tag{27}$$

This solution also applies to the single-dish RAS. Next, substituting (27) to (24), the approximated mean μ_ρ of the estimated astronomical source power is

$$\mu_\rho = \mathbb{E}[\mu_{\rho|\mathcal{E}}] \approx \sigma_{\rm s}^2 \tag{28}$$

where the approximation is due to the assumption $\mathbb{E}\left[|e_{\rm t}^i(n)|^2\right] = \mathbb{E}\left[|e_{\rm r}^i(n)|^2\right]$ since $\sigma_{\rm s}^2 \ll \sigma_{\rm n}^2$. Substituting (27) to (25), we obtain the variance $\sigma_{\rm array}^2$ of the estimated astronomical source power as in (29) shown at the bottom of next page. The first approximation in (29) holds because

$$\mathrm{Var}(\mathbb{E}[\rho_{\rm array}|\mathcal{E}]) = \mathbb{E}\left[\sigma_{\rm s}^2 + \frac{\mathrm{MSE_t}(L)}{ML} - \frac{\mathrm{MSE_r}(L)}{ML}\right]^2 - \sigma_{\rm s}^4 \approx 0. \tag{30}$$

The second approximation in (29) is due to $\sigma_{\rm s}^2 \ll \sigma_{\rm n}^2$ and $\mathbb{E}\left[|e_{\rm t}^i(n)|^2\right] \ll \sigma_{\rm n}^2$.

Similarly, we can also obtain approximate results for the single-dish RAS. The mean value of the estimated source power is the same as (28) while the variance is

$$\sigma_{\rm single}^2 \approx \frac{2\sigma_{\rm n}^4}{N}. \tag{31}$$

$$\begin{aligned}
\mathbb{E}\left[\rho_{\rm in}^2\right] &= \frac{1}{M^2L^2}\sum_{i,j=1}^{M}\sum_{n,m=1}^{L}\mathbb{E}\left[\Re\{y_{\rm t}^i(n)\}^2\Re\{y_{\rm t}^j(m)\}^2 + \Re\{y_{\rm r}^i(n)\}^2\Re\{y_{\rm r}^j(m)\}^2 - 2\Re\{y_{\rm t}^i(n)\}^2\Re\{y_{\rm r}^j(m)\}^2\right] \\
&\overset{(a)}{\approx} \frac{1}{ML}\left\{\mathbb{E}[\Re\{y_{\rm t}^i(n)\}^4] + \mathbb{E}[\Re\{y_{\rm r}^i(n)\}^4] - 2\mathbb{E}[\Re\{y_{\rm t}^i(n)\}^2]\mathbb{E}[\Re\{y_{\rm r}^i(n)\}^2]\right\} \\
&\quad + \frac{ML-1}{ML}\left\{\mathbb{E}\left[\Re\{y_{\rm t}^i(n)\}^2\right] - \mathbb{E}\left[\Re\{y_{\rm r}^i(n)\}^2\right]\right\}^2 \\
&= \frac{1}{ML}(\phi_{\rm t} + \phi_{\rm r} - 2\varphi_{\rm t}\varphi_{\rm r}) + \frac{ML-1}{ML}(\varphi_{\rm t} - \varphi_{\rm r})^2.
\end{aligned} \tag{11}$$

Note that the approximate closed-form results correspond to the scenario with very low SNR (relevant for RAS) and negligible quantization error. Thus, comparison between the exact expressions from the previous section and the approximate ones will reveal the effect of quantization errors on the RAS power estimation performance. To observe this, we define their ratios as the normalized performance metrics as

$$\gamma_\mu \triangleq \frac{\mathbb{E}[\rho_{\text{single}}]}{\mu_\rho} = \frac{\mathbb{E}[\rho_{\text{array}}]}{\mu_\rho} \tag{32}$$

$$\gamma_\sigma \triangleq \frac{\text{Var}(\rho_{\text{single}})}{\sigma^2_{\text{single}}} = \frac{\text{Var}(\rho_{\text{array}})}{\sigma^2_{\text{array}}}. \tag{33}$$

We note that the single-dish RAS and the DART system share the same term of each normalized performance metric and hence we can use variables γ_μ and γ_σ for both systems.

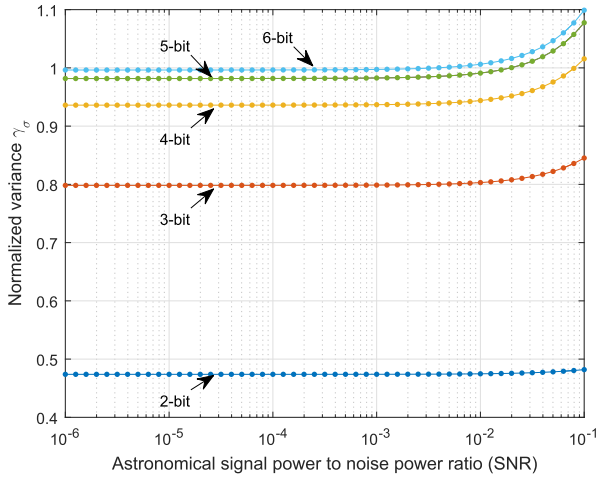

FIGURE 5. The normalized variance of RAS signal power estimation under various ADC resolutions ($\sigma_s^2 = 1$, N or $L = 10^4$).

We present the effect of ADC resolution on the RAS power estimation performance by plotting γ_μ and γ_σ under various ADC resolutions in Fig. 4 and Fig. 5 respectively, where we apply trained Lloyd-Max quantizers corresponding to the noise variance. To verify the analytical results, we conducted Monte Carlo simulations using $\sigma_s^2 = 1$ and SNR $= -20$ dB. TABLE 1 shows the corresponding simulation results which match with the analytical results in Fig. 4 and Fig. 5. From the results in the figures, the following observations are in order:

1) A smaller ADC resolution introduces a larger bias to the mean of the RAS power estimation.
2) To obtain approximately unbiased estimates without additional bias compensation, an ADC resolution of at least 6 bits is needed.
3) The variance of the RAS power estimation reduces with decreasing ADC resolution.
4) The effects of ADC resolution in terms of the estimation mean and variance are approximately constant within the typical SNR range of interest for RAS (< -20 dB). This also allows us to use a small ADC resolution (causing a bias) and then compensate the precomputed bias.

After the bias compensation (i.e., multiplying with $1/\gamma_\mu$), the variance of the unbiased RAS power estimation is given by

$$\gamma_{\sigma,\text{unbiased}} \triangleq \frac{\text{Var}(\rho_{\text{single}}/\gamma_\mu)}{\sigma^2_{\text{single}}} = \frac{\text{Var}(\rho_{\text{array}}/\gamma_\mu)}{\sigma^2_{\text{array}}} = \frac{\gamma_\sigma}{\gamma_\mu^2}. \tag{34}$$

It is crucial for the RAS power estimator to be unbiased and hence, (34) is a more meaningful metric than (33).

Given the two facts, first, the ADC resolution is approximately constant within the typical low SNR range, second, the mean $\mathbb{E}[\rho_{\text{single}}]$ (or $\mathbb{E}[\rho_{\text{array}}]$) and variance $\text{Var}(\rho_{\text{single}})$ (or $\text{Var}(\rho_{\text{array}})$) are proportional to their closed-form approximations μ_ρ and σ^2_{single} (or σ^2_{array}) by factor γ_μ and γ_σ respectively according to (32) and (33), we will mainly use the closed form results σ^2_{single} and σ^2_{array} in the following analysis for representation simplicity.

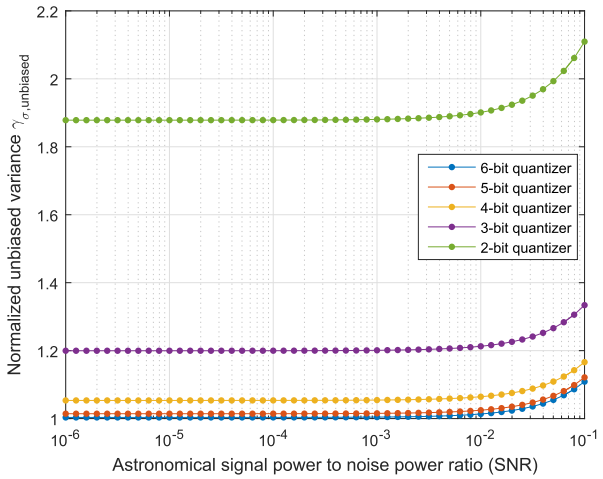

FIGURE 6. The normalized variance of RAS signal power estimation after the bias compensation ($\sigma_s^2 = 1$, N or $L = 10^4$).

Fig. 6 presents the variance of the unbiased RAS power estimator for different ADC resolutions. We can observe that a higher ADC resolution yield a smaller variance. However, the performance saturates for ADC resolution of 6 bits or more. We also simulated 7 and 8 bits ADC resolutions and the results are indistinguishable from that of 6 bits ADC and

$$\begin{aligned}\sigma^2_{\text{array}} &= \mathbb{E}\left[\text{Var}(\rho_{\text{array}}|\mathcal{E})\right] + \text{Var}(\mathbb{E}[\rho_{\text{array}}|\mathcal{E}]) \\ &\approx \frac{2}{ML}\sigma_{\text{n}}^4 + \frac{1}{ML}(2\sigma_s^2\sigma_{\text{n}}^2 + \sigma_{\text{s}}^4) + \frac{2}{ML}(\sigma_{\text{n}}^2 + \sigma_{\text{s}}^2)\mathbb{E}\left[|e_{\text{t}}^i(n)|^2\right] + \frac{2}{ML}\sigma_{\text{n}}^2\mathbb{E}\left[|e_{\text{r}}^i(n)|^2\right] \approx \frac{2\sigma_{\text{n}}^4}{ML}.\end{aligned} \tag{29}$$

TABLE 1. Comparison of different quantization resolutions.

Bits	2	3	4	5	6
Simulated Mean (or γ_μ)	0.4967	0.8106	0.9447	0.9746	0.9986
Simulated Variance	0.9528	1.6165	1.8896	1.9871	2.0089
Corresponding γ_σ	0.4764	0.8082	0.9448	0.9936	1.0044

TABLE 2. Comparison of different numbers of antenna elements.

M	1	10	50
Simulated Mean (or γ_μ)	0.9447	0.9421	0.9402
Simulated Variance	1.8896	0.1896	0.0386
Corresponding γ_σ	0.9448	0.9481	0.9640

hence they are not plotted in Fig. 6 for the sake of clarity of the other curves. And $\gamma_{\sigma,\text{unbiased}}$ converges to 1 as the resolution increases. As a larger ADC resolution yield a higher data rate, trade-offs can be made between data rates and estimation performance. A good choice is 6 bits ADC resolution as more bits do not yield noticeable performance improvement.

Next, we evaluate the effect of the number of antennas. With the settings that $\sigma_s^2 = 1$ and $N = 10^4$, TABLE 2 shows the Monte Carlo simulation results for a 4-bit quantizer at SNR $= -20$ dB when the number of antenna elements varies. Comparing the multi-antenna results to the single antenna result in this table, we observe the following.

1) The variance of estimated power decreases by a factor around M when more antennas are combined. This illustrates a benefit of the DART system.
2) The corresponding normalized metric γ_σ, which in its approximate form in (14) is independent of M, slightly increases with M. This is due to the mismatch between the assumption of independence among the received signals at different antennas in the analysis and the correlation of the received signals across antennas due to the same astronomical signal in the simulation. In other words, the difference between γ_σ for $M > 1$ and γ_σ for $M = 1$ implies how accurate the approximation in (14) is, and the results show good accuracy.
3) The simulation result of γ_μ does not grow with M (thus, maintaining unbiased estimation for different values of M) since the signal correlation does not affect the mean of the estimated power.

V. COMBINATION AND PERFORMANCE COMPARISON BETWEEN DART AND THE SINGLE-DISH RAS

Here, we evaluate the performance of the DART by incorporating specifics of the coexistence paradigm and then compare it with the performance of the single-dish RAS (the isolation paradigm). Recall the system parameters for the shared spectrum access described in Section II. Suppose the hourly allocation of the number of subframes per frame to the three phases is pre-designed according to the CWC traffic statistics as in [15]. Let $n_{\text{array},l}$ denote the number of subframes per frame allocated to the DARTs for the lth hour. An example of available observation intervals of DART in terms of $n_{\text{array},l}$ is shown by a line curve in Fig. 8 based on the system setting in [15]. DART is allocated with longer (shorter) observation intervals during hours with lower (higher) CWC average traffic loads. Thus, the hourly estimation performance of DART would vary as well.

The number of samples at hour l for DART is given by $2L_l = 2Bn_{\text{array},l}\tau_{\text{sf}}N_{\text{f/hour}}$ while that for the single-dish RAS is $2N = 2Bn_{\text{f}}\tau_{\text{sf}}N_{\text{f/hour}}$ at any hour. Then, the variances of the estimated powers in (29) and (31) for hour l are

$$\sigma^2_{\text{array},l} \approx \frac{2\sigma_{\text{n}}^4}{MBn_{\text{array},l}\tau_{\text{sf}}N_{\text{f/hour}}}, \quad l = 1, \ldots, 24 \tag{35}$$

$$\sigma^2_{\text{single},l} = \frac{2\sigma_{\text{n}}^4}{Bn_{\text{f}}\tau_{\text{sf}}N_{\text{f/hour}}}, \quad l = 1, \ldots, 24. \tag{36}$$

As hourly based signal power estimates denoted by $\{\rho_{\text{array},l}\}$ have different accuracies, if the desired power estimation needs to be computed over K hours $(l_1, \ldots, l_K)$, we can apply the best linear unbiased estimation [30] to combine the K estimates as

$$\rho_{\text{array}} = \sum_{k=1}^{K} \beta_k \rho_{\text{array},l_k} \tag{37}$$

where

$$\beta_k = \frac{1/\sigma^2_{\text{array},l_k}}{\sum_{n=1}^{K} 1/\sigma^2_{\text{array},l_n}} \tag{38}$$

minimizes the variance of combined estimation $\sigma^2_{\text{array}} \approx \sum_{k=1}^{K} \beta_k^2 \sigma^2_{\text{array},l_k}$, under the unbiased constraint $\sum_{k=1}^{K} \beta_k = 1$. The approximation is due to the assumption that observations in different hours are regarded to be independent since noise is the dominant received signal. Thus, the corresponding estimator variance for the DART system is given by

$$\sigma^2_{\text{array}} \approx \frac{2\sigma_{\text{n}}^4}{MB\tau_{\text{sf}}N_{\text{f/hour}}\sum_{k=1}^{K} n_{\text{array},l_k}}. \tag{39}$$

We notice that (39) indicates this estimator variance is equivalent to the variance achieved by averaging all the samples in K hours. Meanwhile, we denote r as the ratio of the total resources allocated over the above K hours between CWC and RAS, i.e., $r = (\sum_{k=1}^{K} n_{\text{CWC},l_k})/(\sum_{k=1}^{K} n_{\text{RAS},l_k})$. A comparison between the variance achieved by the BLUE approach and the variance achieved by simply averaging $\sigma^2_{\text{array},l}$, $l = 1, \ldots, K$ for different values of the resource ratio r is shown in Fig. 7. It can be observed that in a feasible range of the ratio r, the BLUE combining approach always outperforms the simple averaging method in terms of the variance of the estimated power.

For the single-dish RAS, we can simply average the K estimates as $\rho_{\text{single}} = \sum_{k=1}^{K} \rho_{\text{single},l_k}/K$ and the corresponding variance is

$$\sigma^2_{\text{single}} = \frac{2\sigma_{\text{n}}^4}{KBn_{\text{f}}\tau_{\text{sf}}N_{\text{f/hour}}}. \tag{40}$$

In a typical deployment of the shared spectrum access, a fixed minimum value of $n_{\text{CWC+RAS},l} = n_{\text{CWC+RAS}}$ would

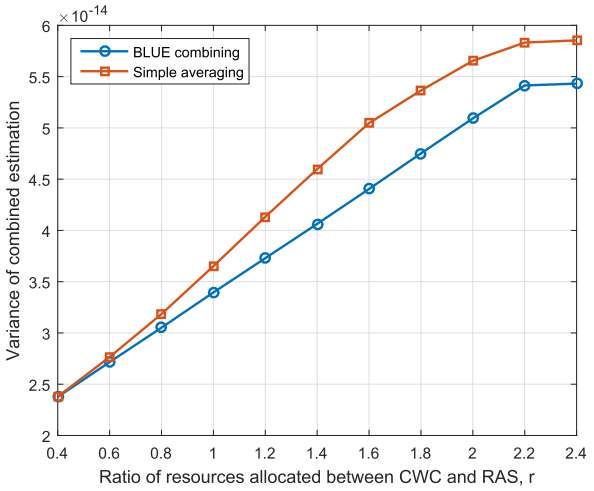

FIGURE 7. Comparison between BLUE and simple averaging.

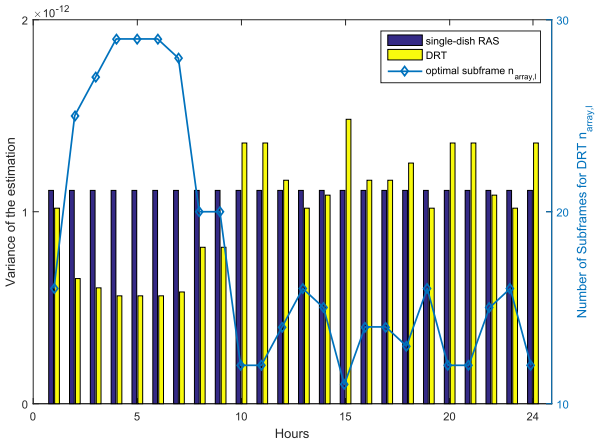

FIGURE 8. Accuracy performance comparison and optimal subframe numbers.

be used across time to maximize the spectrum utilization. Then, with $\eta \triangleq (n_{\rm f} - n_{\rm CWC+RAS})/n_{\rm f}$, we have

$$\sum_{k=1}^{K} n_{{\rm array},l_k} = \frac{\eta K}{1+r} n_{\rm f}. \tag{41}$$

Next, from (39), (40) and (41), we obtain

$$\sigma^2_{\rm array} \approx \frac{1+r}{M\eta}\sigma^2_{\rm single}. \tag{42}$$

The above equation shows the relationship between the estimation accuracy of the DART system and that of the single-dish RAS. For example, to achieve the same or better estimation performance than the single-dish RAS with a radio quiet zone, the DART system needs at least $M = \lceil \frac{1+r}{\eta} \rceil$ antenna elements coexisting with CWC.

To compare the estimation accuracy of different systems, we assume that $\sigma^2_{\rm n} = 1$, $K = 24$, $B = 500$MHz, $\tau_{\rm sf} = 38.5\mu s$, $n_{\rm f} = 44$, $n_{\rm CWC+RAS} = 4$ and $r = 1.25$. Then, we have $M = \lceil \frac{1+r}{\eta} \rceil = 3$. Next, according to the $n_{{\rm array},l}$ curve shown in Fig. 8, the variances of estimated power in each hour are computed and also presented in Fig. 8. Clearly, the variance of estimated power of the DART system is inversely proportional to the number of allocated subframes while the single-dish RAS's variance remains a constant value. Combining all the estimates by the best linear unbiased estimation, we find the corresponding variances for the DART system and the single-dish RAS are $\sigma^2_{\rm array} = 3.82 \times 10^{-14}$ and $\sigma^2_{\rm single} = 4.63 \times 10^{-14}$, respectively. Therefore, with enough numbers of DARTs, the DART system can outperform the single-dish RAS in terms of overall estimation accuracy even though it may have worse performance in some estimation periods.

Furthermore, instead of using the single-dish RAS and the DART system separately, we combine the DART system with the single-dish RAS so that the overall performance can be enhanced. In this scenario, the two systems observe the same astronomical source from different locations and the DART is regarded as an auxiliary system which provides additional observation samples. In particular, since the astronomical signal is significantly weaker than the noise, we assume the estimated astronomical powers of both systems are uncorrelated, i.e., $\rho_{\rm single}$ and $\rho_{\rm array}$ are uncorrelated. According to the BLUE approach, the combined estimation is

$$\bar{\rho} = \theta\rho_{\rm single} + (1-\theta)\rho_{\rm array} \tag{43}$$

where $\theta = \frac{\sigma^2_{\rm array}}{\sigma^2_{\rm single}+\sigma^2_{\rm array}}$. Therefore, the variance of combined estimation is

$$\bar{\sigma}^2 = \frac{\sigma^2_{\rm single}\sigma^2_{\rm array}}{\sigma^2_{\rm single}+\sigma^2_{\rm array}}. \tag{44}$$

Specifically, applying previous system settings, $\sigma^2_{\rm array} = 3.82 \times 10^{-14}$ and $\sigma^2_{\rm single} = 4.63 \times 10^{-14}$, we have $\bar{\sigma}^2 = 2.09 \times 10^{-14}$, which implies with the assistance of a 3-DART system, the single-dish RAS estimation variance can be reduced by more than half.

VI. AVERAGE PERFORMANCE UNDER COOLING POWER CONSTRAINT

The accuracy of radio astronomical observation is largely dependent on the noise level of the receiver. To achieve higher observation accuracy, noise should be mitigated as much as possible. A common physical method is cooling the hardware down to an acceptable low temperature since thermal noise is the most dominant noise in the receiver. The cooling process consumes a significant part of energy of the whole radio astronomy telescope [31] which motivates us to investigate the power efficiency of the DART system.

A. DART PERFORMANCE ANALYSIS

In this section, we consider that K astronomical observations to the same object are conducted hourly and aim to minimize the estimation variance based on the K observation periods. Since the cooling process consumes a substantial part of energy, we propose an dynamic cooling power allocation

approach to optimize the cooling temperature under a total cooling power constraint.

The noise variance at hour l_k can be represented in terms of noise temperature T_{l_k} as

$$\sigma^2_{\mathrm{n},l_k} = \kappa T_{l_k} B \tag{45}$$

where $\kappa = 1.3807 \times 10^{-23}$ is the Boltzmann constant and B is the noise bandwidth. With (35) and (45), the variances of estimated power are given as

$$\sigma^2_{\mathrm{array},l_k} = \frac{2(\kappa T_{l_k} B)^2}{MBn_{\mathrm{array},l_k}\tau_{\mathrm{sf}} N_{\mathrm{f/hour}}} = \frac{\alpha T^2_{l_k}}{Mn_{\mathrm{array},l_k}} \tag{46}$$

where constant $\alpha = \frac{2\kappa^2 B}{\tau_{\mathrm{sf}} N_{\mathrm{f/hour}}}$. Furthermore, the average variance of the estimated powers in K hours is $\frac{1}{K}\sum_{k=1}^{K} \frac{\alpha T^2_{l_k}}{Mn_{\mathrm{array},l_k}}$.

According to (46), in order to achieve a desired variance of the estimation, radio astronomical receivers should be cooled down to certain low temperatures to mitigate the thermal noise. Lower temperature results in higher estimation accuracy but also indicates higher power consumption. Thus, given a certain amount of power and the time varying nature of the ambient temperature, dynamically allocating the power to optimize the cooling temperature will be more preferable than the conventional approach which maintains a fixed temperature.

Assuming an idealized scenario where there is no thermodynamic loss, the second law of thermodynamics connects the minimum required power P_{MIN} to cool down a surface from ambient temperature T_{amb} to a desired temperature T_0 in the form of Carnot equation [32],

$$P_{\mathrm{MIN}} = \frac{T_{\mathrm{amb}} - T_0}{T_0} \cdot Q_0 \tag{47}$$

where Q_0 is called cooling capacity[4] [32].

In the following parts of this section, we assume that 1) the DARTs observes the same astronomical source signal for K hours, 2) both the CWC traffic statistics and the ambient temperature (statistics) vary hourly and are known in advance, 3) the receiver's temperature can be cooled down from ambient temperature T_{amb,l_k} to any achievable temperature T_{l_k} in hour l_k, 4) the system has a constant cooling capacity Q_0, and 5) all the K observations are combined linearly with weighting parameter β_k to improve the estimation performance. Thus, the variance of the combined estimation is written as

$$\sigma^2_{\mathrm{array}} = \sum_{k=1}^{K} \beta_k^2 \sigma^2_{\mathrm{array},l_k}. \tag{48}$$

Then, our problem is formulated as a joint optimization problem over the weighting parameters $\{\beta_k\}$ and the feasible cooling temperatures $\{T_{l_k}\}$ under the total cooling power constraint,

$$\begin{aligned} \text{(P0):} \quad \min_{\{T_{l_k}\},\,\{\beta_k\}} \quad & \sum_{k=1}^{K} \beta_k^2 \frac{\alpha T^2_{l_k}}{Mn_{\mathrm{array},l_k}} \\ \text{s.t.} \quad & \sum_{k=1}^{K} \left(\frac{T_{\mathrm{amb},l_k}}{T_{l_k}} - 1\right) Q_0 \le P \\ & T_{\min} \le T_{l_k} \le T_{\mathrm{amb},l_k} \\ & \sum_{k=1}^{K} \beta_k = 1, \quad \beta_k \ge 0 \end{aligned} \tag{49}$$

where $T_{\min}$ is the minimum achievable receiver temperature of the cooling system and P is the sum of available cooling powers over K hours for an antenna. We also note that in the second constraint of (49), the upper bound T_{amb,l_k} can be replaced by any feasible maximum temperature constraint smaller than the ambient temperature.

Problem (P0) has convex constraints but non-convex objective function with respect to both $\{T_{l_k}\}$ and $\{\beta_k\}$. However, (P0) can be verified to be convex over either $\{T_{l_k}\}$ or $\{\beta_k\}$ if the other optimization variable is fixed. Therefore, we apply an alternating optimization approach to iteratively find the optimal values of $\{T_{l_k}\}$ and $\{\beta_k\}$. Specifically, let $\left(T^{(n)}_{l_k}, \beta^{(n)}_k\right)$ denote the solutions at the nth iteration, the solution of (P0) can be obtained by alternatively solving the following two convex optimization problems,

$$\begin{aligned} \text{(P1-1):} \quad \{T^{(n)}_{l_k}\} = \arg\min_{\{T_{l_k}\}} \quad & \sum_{k=1}^{K} \left(\beta_k^{(n-1)}\right)^2 \frac{\alpha T^2_{l_k}}{Mn_{\mathrm{array},l_k}} \\ \text{s.t.} \quad & \sum_{k=1}^{K} \left(\frac{T_{\mathrm{amb},l_k}}{T_{l_k}} - 1\right) Q_0 \le P \\ & T_{\min} \le T_{l_k} \le T_{\mathrm{amb},l_k} \end{aligned} \tag{50}$$

and

$$\begin{aligned} \text{(P1-2):} \quad \{\beta^{(n)}_k\} = \arg\min_{\{\beta_k \ge 0\}} \quad & \sum_{k=1}^{K} \beta_k^2 \frac{\alpha \left(T^{(n)}_{l_k}\right)^2}{Mn_{\mathrm{array},l_k}} \\ \text{s.t.} \quad & \sum_{k=1}^{K} \beta_k = 1. \end{aligned} \tag{51}$$

The solution to (P1-2) can be easily obtained as

$$\beta^{(n)}_k = \frac{1/\pi^{(n)}_k}{\sum_{l=1}^{K} 1/\pi^{(n)}_l} \tag{52}$$

where $\pi^{(n)}_k \triangleq \frac{\alpha (T^{(n)}_{l_k})^2}{Mn_{\mathrm{array},l_k}}$. Next, we can state the following propositions.

Proposition 1: The approach of alternatively solving (P1-1) and (P1-2) is convergent.

Proof: Since both (P1-1) and (P1-2) are convex optimization problems, this approach can be regarded as a special case of the two-block Gauss-Seidel method whose convergence is proved in [34]. □

[4]Cooling capacity is the measure of a cooling system's ability to remove heat [33].

Proposition 2: Defining $\omega_{l_k} \triangleq \frac{T_{\text{amb},l_k}}{T_{l_k}}$, *the following two optimization problems have the same solution in terms of the cooling temperatures* $\{T_{l_k}\}$*: i) Alternatively solving (P1-1) and (P1-2), and ii) (P2) which is constructed as*

$$\begin{aligned} \text{(P2):} \quad & \max_{\{\omega_{l_k}\}} \sum_{k=1}^{K} \frac{n_{\text{array},l_k}}{T^2_{\text{amb},l_k}} \omega^2_{l_k} \\ & \text{s.t.} \sum_{k=1}^{K} \omega_{l_k} \le \tilde{P} \\ & 1 \le \omega_{l_k} \le \frac{T_{\text{amb},l_k}}{T_{\min}} \end{aligned} \tag{53}$$

where $\tilde{P} = \frac{P}{Q_0} + K$.

Proof: The proof is in Appendix. □

With the above two propositions, the solution to (P2) in terms of cooling temperature $\{T_{l_k}\}$ can also be a near-optimal solution to the original problem (P0). Besides, the corresponding weighting parameter $\{\beta_k\}$ can be computed by (52).

Remark 1: We can verify that (P2) is not a convex optimization problem since it aims to maximize a convex objective function. However, the two linear constraints fortunately allow us to use simple power allocation algorithms to find the optimal solution. Specifically, the first constraint of (P2) bounds the sum of ω_{l_k}'s while the second constraint provides the lower and upper bounds for individual ω_{l_k}'s. On the other hand, the objective function is a weighted sum of $\omega^2_{l_k}$ where the non-negative weighting parameter is known. Therefore, it is always preferable to allocate as much power[5] to the l_ith element ω_{l_i} where $i = \arg\max_k \frac{n_{\text{array},l_k}}{T^2_{\text{amb},l_k}}$. Thus the optimal solution to (P2) for the kth hour can only be chosen from three values, the minimum value 1, the maximum value $\frac{n_{\text{array},l_k}}{T^2_{\text{amb},l_k}}$ or a certain value between the minimum and maximum. Likewise, only one of the three cooling temperatures at the kth hour can be selected as the solution to alternatively solving (P1-1) and (P1-2), and they are the minimum achievable cooling temperature $T_{\min}$, the ambient temperature T_{amb,l_k} (i.e., the cooling system is off) and a certain temperature between these two (i.e., when the residual cooling power is not enough to cool the receiver down to $T_{\min}$).

Now, we summarize the above analysis for solving (P2) in Algorithm 1.

Adopting previous simulation settings together with $Q_0 = 100W$, $T_{\min} = 60$ Kelvin, $T_{\text{amb},l_k} = 286, 285, 283, 282, 279, 282, 285, 289, 292, 295, 297, 298, 299, 300, 301, 302, 301, 300, 297, 294, 291, 290, 289, 288$ Kelvin for $k = 1, \ldots, 24$, the cooling temperatures solutions under different cooling power constraints are shown in Fig. 9. To be specific, the first figure in Fig. 9 shows the value of $\frac{n_{\text{array},l_k}}{T^2_{\text{amb},l_k}}$ for $k = 1, \ldots, 24$. We can see as the total cooling power P increases from 24dBW to 38dBW, the number of times the minimum cooling temperature is achieved increases. And the cooling power allocation priority corresponds to the increasing order of $\frac{n_{\text{array},l_k}}{T^2_{\text{amb},l_k}}$.

[5]Here we regard $\tilde{P}$ as power for convenience since $\tilde{P}$ is a power related factor.

Algorithm 1 Cooling Power Allocation Algorithm for Problem (P2)

1: Initialize residual power $\tilde{P}' = \tilde{P}$, index set $\mathcal{K} = \{1, \ldots, K\}$, and $\omega_{l_k} = 0$, $\forall k \in \mathcal{K}$,
2: Allocate 1 unit of power to satisfy the lower bound constraint of $\{\omega_{l_k}\}$ in the second constraint of (P2), renew the residual power $\tilde{P}' = \tilde{P} - K$;
3: **while** $\tilde{P}' > 0$ **do**
4: Next power allocation index $i = \arg\max_{k\in\mathcal{K}} \frac{n_{\text{array},l_k}}{T^2_{\text{amb},l_k}}$, renew $\mathcal{K} = \mathcal{K}\backslash i$;
5: **if** $\tilde{P}' \ge \frac{n_{\text{array},l_i}}{T^2_{\text{amb},l_i}} - 1$ **then**
6: $\omega_{l_i} = \frac{n_{\text{array},l_i}}{T^2_{\text{amb},l_i}}$, renew $\tilde{P}' = \tilde{P}' - (\frac{n_{\text{array},l_i}}{T^2_{\text{amb},l_i}} - 1)$;
7: **else**
8: $\omega_{l_i} = \tilde{P}' + 1$, renew $\tilde{P}' = 0$;
9: **end if**
10: **end while**
11: Output $\{\omega_{l_k}\}_{k=1}^{K}$.

To evaluate the power saving of this approach, we can consider the scenario where the DART system always maintains a fixed cooling temperature T_{array} no less than $T_{\min}$ by default setting and has the same cooling power constraint P at each antenna. Then, similar to the first constraint of (49), we have

$$\sum_{k=1}^{K} \left(\frac{T_{\text{amb},l_k}}{T_{\text{array}}} - 1 \right) Q_0 \le P \tag{54}$$

which results in

$$T_{\text{array}} \ge \max \left\{ T_{\min}, \frac{\sum_{k=1}^{K} T_{\text{amb},l_k} Q_0}{P + KQ_0} \right\}. \tag{55}$$

Thus, the estimation variance of the DART system with a fixed cooling temperature is represented as

$$\left[\sigma^2_{\text{array}}\right]_{\text{fixed}} = \sum_{k=1}^{K} \beta_k^2 \sigma^2_{\text{array},l_k} \Big|_{\beta_k = \frac{1}{K}} = \sum_{k=1}^{K} \frac{1}{K^2} \frac{\alpha T^2_{\text{array}}}{M n_{\text{array},l_k}} \tag{56}$$

according to (46). Similarly, to compare with the DART system with M antennas, the total available cooling power for single-dish RAS is set as $P_{\text{single}} = MP$ and thus the minimal achievable temperature at cooling capacity Q_0 is

$$T_{\text{single}} \ge \max \left\{ T_{\min}, \frac{\sum_{k=1}^{K} T_{\text{amb},l_k} Q_0}{P_{\text{single}} + KQ_0} \right\}. \tag{57}$$

Therefore, the variance of estimation for the single-dish RAS wth a fixed cooling temperature is represented as

$$\left[\sigma^2_{\text{single}}\right]_{\text{fixed}} = \sum_{k=1}^{K} \beta_k^2 \sigma^2_{\text{single}} \Big|_{\beta_k = \frac{1}{K}} = \frac{1}{K} \frac{\alpha T^2_{\text{single}}}{n_{\text{f}}} \tag{58}$$

according to (40) and the relationship $\sigma^2_{\text{n}} = \kappa T_{\text{single}} B$.

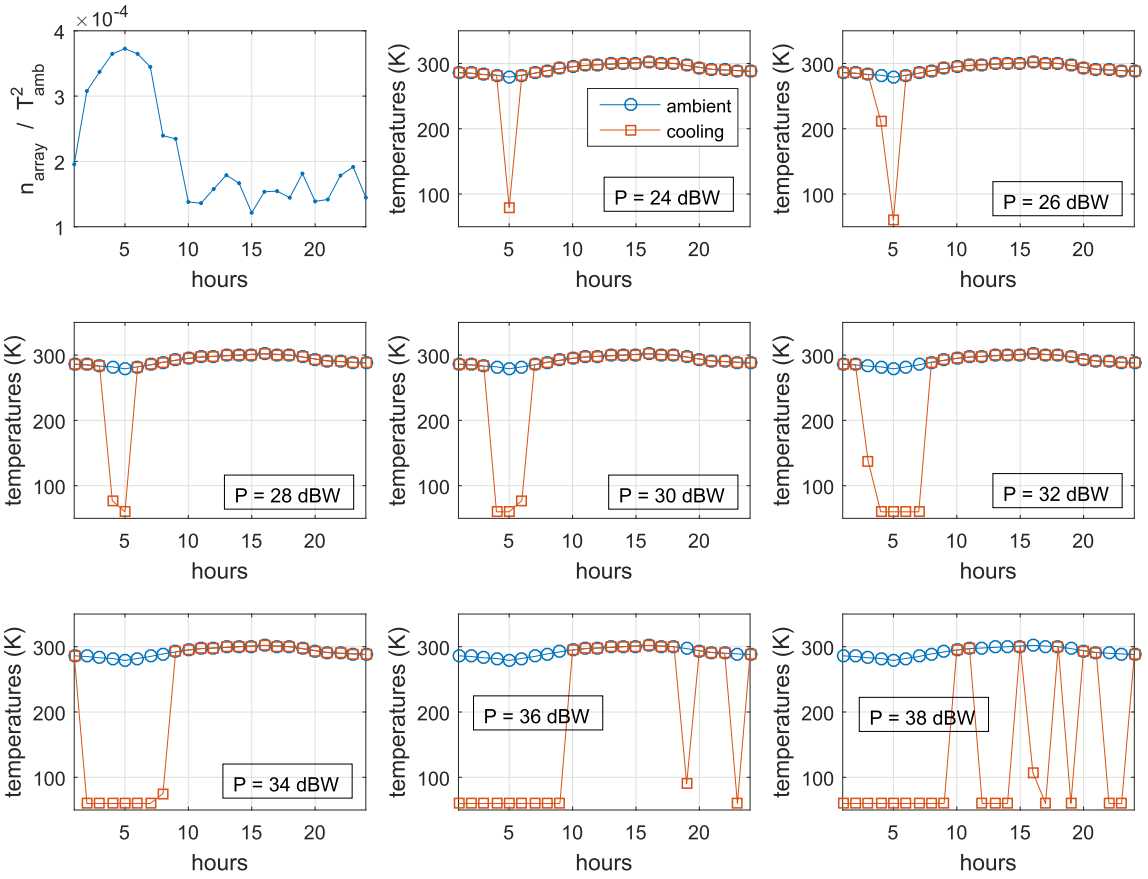

FIGURE 9. Solutions of cooling power allocation in terms of cooling temperatures.

B. IMPERFECT TEMPERATURE INFORMATION

We have assumed that the ambient temperature in each hour are perfectly known for cooling power allocation. However, temperature forecasting may not be perfect and the cooling power requirement in problem (49) may not be satisfied if the temperature is forecast with error. In this scenario, we consider to use a probability constraint on the cooling power shortage. In other words, we suppose that the probability of the required cooling power being larger than the total available power P should be no more than ϵ. To be specific, we assume that the temperature $\mathbf{T} = [T_{\text{amb},l_1}, \ldots, T_{\text{amb},l_K}]^{\mathrm{T}}$ is Gaussian distributed, $\mathbf{T} \sim \mathcal{N}(\boldsymbol{\mu}, \Sigma)$ where the mean values are forecast temperatures $\boldsymbol{\mu} = [\bar{T}_{\text{amb},l_1}, \ldots, \bar{T}_{\text{amb},l_K}]^{\mathrm{T}}$ and the covariance is represented by a Toeplitz matrix Σ. Then, the first constraint of (49) is replaced by

$$\Pr\left[\sum_{k=1}^{K}\left(\frac{T_{\text{amb},l_k}}{T_{l_k}} - 1\right) Q_0 > P\right] \leq \epsilon. \tag{59}$$

Defining $x_{l_k} \triangleq 1/T_{l_k}$, and $\boldsymbol{x} = [x_{l_1}, \ldots, x_{l_K}]^{\mathrm{T}}$, the constraint is rewritten as $\Pr\left(\mathbf{T}^{\mathrm{T}}\boldsymbol{x} > \tilde{P}\right) \leq \epsilon$. Since $\mathbf{T}^{\mathrm{T}}\boldsymbol{x} \sim \mathcal{N}(\boldsymbol{\mu}^{\mathrm{T}}\boldsymbol{x}, \|\Sigma^{\frac{1}{2}}\boldsymbol{x}\|_2)$, (59) is further represented as a second order cone constraint

$$\boldsymbol{\mu}^{\mathrm{T}}\boldsymbol{x} + Q^{-1}(\epsilon)\|\Sigma^{\frac{1}{2}}\boldsymbol{x}\|_2 \leq \tilde{P} \tag{60}$$

where $Q^{-1}(\cdot)$ is the inverse function of the Q function. Therefore, the average performance optimization problem under imperfect temperature information is formulated as the following problem

$$\begin{aligned}(\text{P3}): \quad \min_{\boldsymbol{x},\,\{\beta_k\}} \quad & \sum_{k=1}^{K} \beta_k^2 \frac{\alpha}{M n_{\text{array},l_k} x_{l_k}^2} \\ \text{s.t.} \quad & \boldsymbol{\mu}^{\mathrm{T}}\boldsymbol{x} + Q^{-1}(\epsilon)\|\Sigma^{\frac{1}{2}}\boldsymbol{x}\|_2 \leq \tilde{P} \\ & \frac{1}{\bar{T}_{\text{amb},l_k}} \leq x_{l_k} \leq \frac{1}{T_{\min}} \\ & \sum_{k=1}^{K} \beta_k = 1, \quad \beta_k \geq 0. \end{aligned} \tag{61}$$

We can observe that the modified power constraint will be reduced to the original power constraint in (49) if the temperatures are perfectly forecast as all elements in the covariance Σ would be zero. For the same power constraint, larger covariance or tighter probability constraint can result in smaller $\{x_{l_k}\}$ and therefore larger estimation variance. Likewise, the proposed alternating approach can be used to solve (P3). However, since the total cooling power constraint of (P3) is modified due to the uncertainty of ambient temperatures, the proposed power allocation strategy in Algorithm 1 is not applicable. To handle this problem, we use the convex optimization toolbox CVX [35]. Defining the variance of the

nth iteration as $\left[\sigma^2_{\text{array}}\right]^{(n)} \triangleq \sum_{k=1}^{K} \beta_k^{(n)2} \frac{\alpha (T_{l_k}^{(n)})^2}{M n_{\text{array},l_k}}$ and the counterpart of (P1-1) for the imperfect temperature forecast scenario as

$$\begin{aligned} \text{(P3-1)}: \quad \{x_{l_k}^{(n)}\} = \ & \arg\min_{x_{l_k}} \ \sum_{k=1}^{K} \left(\beta_k^{(n-1)}\right)^2 \frac{\alpha}{M n_{\text{array},l_k} x_{l_k}^2} \\ & \text{s.t.} \ \ \boldsymbol{\mu}^{\mathrm{T}} \boldsymbol{x} + Q^{-1}(\epsilon) \| \Sigma^{\frac{1}{2}} \boldsymbol{x} \|_2 \le \tilde{P} \\ & \frac{1}{\bar{T}_{\text{amb},l_k}} \le x_{l_k} \le \frac{1}{T_{\min}}, \end{aligned} \tag{62}$$

the following Algorithm 2 illustrates the proposed alternating optimization approach to find the cooling power allocation solution for imperfect temperature information scenarios.

Algorithm 2 Cooling Power Allocation Algorithm for Problem (P3)

1: Initialize $n = 1$, $\varepsilon > 0$, $\left[\sigma^2_{\text{array}}\right]^{(0)} = 2\varepsilon$, $\left[\sigma^2_{\text{array}}\right]^{(1)} = \varepsilon$ and $\beta_k^{(0)} = \frac{1}{K}$, $\forall k = 1, \ldots, K$
2: **while** $\left(\left[\sigma^2_{\text{array}}\right]^{(n-1)} - \left[\sigma^2_{\text{array}}\right]^{(n)}\right) / \left[\sigma^2_{\text{array}}\right]^{(n-1)} > \varepsilon$ **do**
3: Solve (P3-1) with CVX, obtain $\{x_{l_k}^{(n)}\}$ and compute $\beta_k^{(n)} = \frac{1/\pi_k^{(n)}}{\sum_{l=1}^{K} 1/\pi_l^{(n)}}$, $k = 1, \ldots, K$;
4: n = n + 1;
5: **end while**
6: Output $\{x_{l_k}^{(n)}\}$ and $\{\beta_k^{(n)}\}$.

C. COMBINATION OF DART AND SINGLE-DISH RAS

We have proposed a DART system that can achieve an estimation performance as accurate as the conventional single-dish RAS. Now, a two-step approach to combine the observations of both systems is proposed to achieve the minimum estimation variance of the K independent observations: 1) the single-dish RAS and the DART system observe separately where the DART apply the estimation optimization approach to obtain the minimum estimation variance and the optimal cooling temperature, 2) the best linear unbiased estimation (BLUE) approach is applied to combine the two estimations from the single-dish RAS and the DART system, using the same weighting parameter θ as shown in (43). In particular, since the astronomical signal is significantly weaker than the noise, we assume the estimated signals of both systems are uncorrelated, i.e., ρ_{single} and ρ_{array} are uncorrelated. Using the BLUE approach as in (43), the variance of combined estimated power is $\bar{\sigma}^2 = \frac{\sigma^2_{\text{single}} \sigma^2_{\text{array}}}{\sigma^2_{\text{single}} + \sigma^2_{\text{array}}}$, where $\sigma^2_{\text{array}} = \sum_{k=1}^{K} \beta_k^2 \sigma^2_{\text{array},l_k}$ is the variance of estimation for the DART system according to (48).

D. SIMULATIONS

In the simulation, we set that 1) for the imperfect temperature information scenarios, $\bar{T}_{\text{amb},l_k} = 286, 285, 283, 282, 279, 282, 285, 289, 292, 295, 297, 298, 299, 300, 301, 302, 301, 300, 297, 294, 291, 290, 289, 288$ Kelvin for $k = 1, \ldots, 24$ respectively, Σ is set to be a symmetric Toeplitz matrix whose first row is [30, 28.75, 27.5, 26.25, 25, 23.75, 22.5, 21.25, 20, 18.75, 17.5, 16.25, 15, 15.75, 16.5, 17.25, 18, 18.75, 19.5, 20.25, 21, 21.75, 22.5, 23.25] and 2) for the perfect temperature information scenarios, $T_{\text{amb},l_k} = \bar{T}_{\text{amb},l_k}$, $\forall k$. Other settings are adopted from previous sections and are the same for both scenarios.

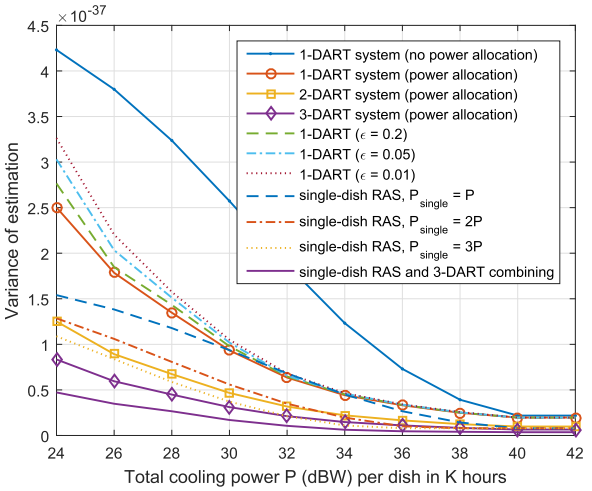

FIGURE 10. Radio astronomical signal power estimation variance comparison among different strategies.

Fig. 10 compares the average variances of the radio astronomical signal power estimation achieved by different strategies, namely, DART without power allocation (fixed cooling temperature), DART with power allocation, DART with power allocation and imperfect ambient temperature information, single-dish RAS (fixed cooling temperature) and the combination of single-dish RAS and DART's estimation, under total cooling power constraint for each DART ranging from 24 dBW to 42 dBW. First of all, we can observe that with increasing cooling power, the variances decrease, and the difference between DART with power allocation and that without power allocation converges to a very small value since all the temperatures are cooled down to the minimum achievable temperature $T_{\min}$. We also mention that the gap between the variance achieved by the two strategies cannot converge to zero since the proposed power allocation contains the BLUE procedure which outperforms the simple averaging of the different estimations, unless n_{array,l_k} is a constant for K hours. This implies our proposed power allocation strategy preforms better, especially in a power limited regime. Also, the relationship among the DART system with different numbers of antennas ($M = 1, 2, 3$) is shown in this figure. As the number of antennas increases from 1 to M, the variance reduces to $1/M$ times of the original value.

Fig. 10 also shows the variances achieved by single-dish RAS with the cooling power allocation strategy under different cooling power constraints. The three different P_{single} are set to compare with the DART system with different numbers of antennas. It can be observed that larger P_{single} corresponds to smaller variance. However, the decrease of the variance becomes remarkable when P_{single} increases. When

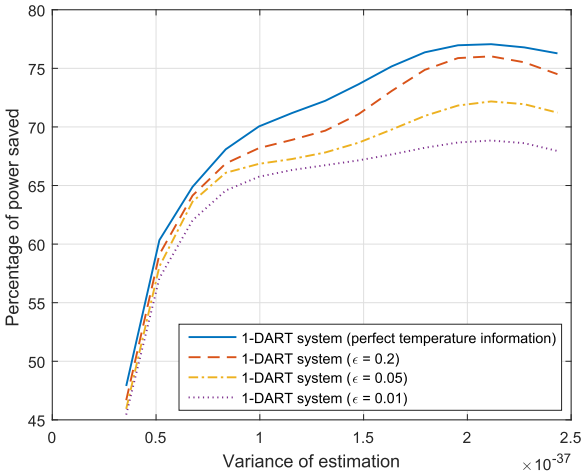

FIGURE 11. Percentage of power saved by the proposed dynamic cooling power allocation.

$M = 1$ ($P_{\text{single}} = P$) and $M = 2$ ($P_{\text{single}} = 2P$), the variances achieved by single-dish RAS are less than those of 1-DART and 2-DART system respectively. While the number of antennas in DARTs increases to 3 ($P_{\text{single}} = 3P$), the variances of 3-DART system are less than those of single-dish RAS for most of the cooling power constraints. This observation indicates the combination of more DARTs with dynamic cooling power allocation will result in higher power efficiency than the single-dish RAS with fixed cooling temperature strategy.

Besides, the bottom curve in Fig. 10 shows the power estimation variance achieved by combining both the single-dish RAS ($P_{\text{single}} = 3P$) and the 3-dish DART system. Obviously, combining the observations of the two systems results in a smaller estimation variance than just applying individual system. For instance, the variance of combined estimation power is as small as half of the variance achieved by the single-dish RAS. These comparisons also imply our proposed DART system can significantly improve the accuracy performance (in terms of estimation variance) of the current RAS systems.

For imperfect ambient temperature information scenarios, three probability constraints are simulated and shown in Fig. 10. Compared with the scenario where ambient temperatures are perfectly forecast, the uncertainty results in higher variance, and tighter probability constraint corresponds to higher variance.

Fig. 11 shows the percentage of power saved by this strategy for certain achieved average variances according to the curves in Fig. 10. We notice that the percentage can be as high as 77 for our system settings. For imperfect temperature information scenarios, to achieve certain variances while guaranteeing a smaller probability of cooling power outage, i.e., from $\epsilon = 0.2$ to $\epsilon = 0.01$, the power saving rate decreases.

VII. CONCLUSION

We have proposed a DART system to embrace the geographical and spectral coexistence between CWC and RAS, and to enhance the capability or performance of RAS. Under the time-division based shared spectrum access, not only RFI-free spectrum access is available to DART during predesigned time slots, but also more DARTs can be deployed without requiring radio quiet zones. We have derived the theoretical performance analysis of the RAS signal power estimation under different ADC resolutions and their closed-form approximations for both the DART system without radio quiet zone and the single-dish RAS with radio quiet zone. Different ADC resolutions introduce different biases to the RAS power estimation but the bias compensation is feasible. With the bias compensation, higher ADC resolution offers the better performance in terms of estimation variance but results in higher data rate. However, the performance saturates for ADC resolution of 6 bits or more. By exploiting more DARTs, the proposed DART system can perform as accurate as (or better than) the conventional single-dish RAS.

Moreover, our proposed dynamic cooling power allocation approach for perfect temperature information scenarios results in a neat solution that always sets the receiver at the minimum cooling temperature for as many duration as possible in a precomputed order of the durations. Under our specific system settings, there is a power saving as much as 77% comparing to the previous method that simply maintains a fixed cooling temperature. Meanwhile, the proposed DART approach has higher power efficiency than the single-dish RAS when the number of antennas increases. For imperfect temperature information scenarios, our alternative optimization approach achieves similar results to those of perfect temperature information scenarios as well as significant power savings. We have also illustrated that when DART and single-dish RAS are combined, further performance improvements achieved.

APPENDIX
PROOF OF PROPOSITION 2

Assuming the alternatively solving (P1-1) and (P1-2) converges at the $\bar{n}$th iteration according to Proposition 1, we have $T_{l_k}^{(\bar{n})} = T_{l_k}$. Then, substituting $\beta_k^{(n-1)} = \beta_k^{(\bar{n})} = \frac{1/\pi_k^{(\bar{n})}}{\sum_{l=1}^{K} 1/\pi_l^{(\bar{n})}}$, $\pi_k^{(\bar{n})} \triangleq \frac{\alpha(T_{l_k}^{(\bar{n})})^2}{M n_{\text{array},l_k}}$ and $T_{l_k}^{(\bar{n})} = T_{l_k}$ to the objective function of (P1-1), the objective can be simplified to

$$\min_{\{T_{l_k}\}} \quad \frac{\alpha}{M} \frac{1}{\sum_{k=1}^{K} \frac{n_{\text{array},l_k}}{T_{l_k}^2}} \tag{63}$$

which is equivalent to maximizing the denominator term and the problem is simplified to

$$\begin{aligned} \max_{\{T_{l_k}\}} \quad & \sum_{k=1}^{K} \frac{n_{\text{array},l_k}}{T_{l_k}^2} \\ \text{s.t.} \quad & \sum_{k=1}^{K} \left(\frac{T_{\text{amb},l_k}}{T_{l_k}} - 1 \right) Q_0 \le P \\ & T_{\min} \le T_{l_k} \le T_{\text{amb},l_k}. \end{aligned} \tag{64}$$

Next, substituting $T_{l_k} \triangleq \frac{T_{\text{amb},l_k}}{\omega_{l_k}}$ and $\tilde{P} = \frac{P}{Q_0} + K$ to this problem, (64) will be further simplified to problem (P-2)

defined in the Proposition 2. In summary, beginning with the convergence condition of alternatively solving (P1-1) and (P1-2), we transfer the alternating optimization problem to a single variable optimization problem (64) which is equivalent to (P-2), hence, proving Proposition 2.

ACKNOWLEDGMENT

Part of this paper will be presented at GLOBECOM 2017 [1].

REFERENCES

[1] D. Han and H. Minn, "Performance analysis of distributed radio telescopes under shared spectrum access paradigm," in *Proc. IEEE Global Commun. Conf. (GLOBECOM)*, Dec. 2017, pp. 1–6.
[2] National Research Council, *Spectrum Management for Science in the 21st Century*. Washington, DC, USA: National Academies Press, 2010.
[3] *Protection Criteria Used for Radio Astronomical Measurements*, document ITU Rec. RA. 769-2, ITU-R, Mar. 2003.
[4] National Research Council, *Handbook of Frequency Allocations and Spectrum Protection for Scientific Uses*. Washington, DC, USA: National Academies Press, 2007.
[5] W. van Driel, "Radio quiet, please!—Protecting radio astronomy from interference," *Proc. Int. Astron. Union*, vol. 5, no. S260, pp. 457–464, 2009.
[6] J. G. Andrews *et al.*, "What will 5G be?" *IEEE J. Sel. Areas Commun.*, vol. 32, no. 6, pp. 1065–1082, Jun. 2014.
[7] P. Pritzker and L. E. Strickling, "Fourth interim progress report on the ten-year plan and timetable and plan for quantitative assessments of spectrum usage," US Dept. Commerce, Washington, DC, Jun. 2014. [Online]. Available: https://www.ntia.doc.gov/files/ntia/publications/fourth_interim_progress_report_final.pdf
[8] Z.-Q. Luo and S. Zhang, "Dynamic spectrum management: Complexity and duality," *IEEE J. Sel. Topics Signal Process.*, vol. 2, no. 1, pp. 57–73, Feb. 2008.
[9] R. Q. Hu and Y. Qian, "An energy efficient and spectrum efficient wireless heterogeneous network framework for 5G systems," *IEEE Commun. Mag.*, vol. 52, no. 5, pp. 94–101, May 2014.
[10] Y. Liao, L. Song, Z. Han, and Y. Li, "Full duplex cognitive radio: A new design paradigm for enhancing spectrum usage," *IEEE Commun. Mag.*, vol. 53, no. 5, pp. 138–145, May 2015.
[11] V. Pankonin and R. M. Price, "Radio astronomy and spectrum management: The impact of WARC-79," *IEEE Trans. Electromagn. Compat.*, vol. EMC-23, no. 3, pp. 308–317, Aug. 1981.
[12] *Preferred Frequency Bands for Radio Astronomical Measurements*, document ITU Rec. RA. 314-10, ITU-R, Jun. 2003.
[13] A. R. Thompson, "ITU-R recommendations of particular importance to radio astronomy," in *Proc. Spectr. Manage. Radio Astron.*, vol. 1. 2004, p. 121.
[14] D. Emerson, "Why single-dish?" in *Proc. Single-Dish Radio Astron., Techn. Appl.*, vol. 278. 2002, pp. 27–43.
[15] H. Minn, Y. R. Ramadan, and Y. Dai, "A new shared spectrum access paradigm between cellular wireless communications and radio astronomy," in *Proc. IEEE Global Commun. Conf. (GLOBECOM)*, Dec. 2016, pp. 1–6.
[16] Y. R. Ramadan, H. Minn, and Y. Dai, "A new paradigm for spectrum sharing between cellular wireless communications and radio astronomy systems," *IEEE Trans. Commun.*, vol. 65, no. 9, pp. 3985–3999, Sep. 2017.
[17] I. F. Akyildiz, W.-Y. Lee, M. C. Vuran, and S. Mohanty, "NeXt generation/dynamic spectrum access/cognitive radio wireless networks: A survey," *Comput. Netw.*, vol. 50, no. 13, pp. 2127–2159, 2006.
[18] G. Zhao, G. Y. Li, and C. Yang, "Proactive detection of spectrum opportunities in primary systems with power control," *IEEE Trans. Wireless Commun.*, vol. 8, no. 9, pp. 4815–4823, Sep. 2009.
[19] J. J. Meng, W. Yin, H. Li, E. Hossain, and Z. Han, "Collaborative spectrum sensing from sparse observations in cognitive radio networks," *IEEE J. Sel. Areas Commun.*, vol. 29, no. 2, pp. 327–337, Feb. 2011.
[20] T. Yucek and H. Arslan, "A survey of spectrum sensing algorithms for cognitive radio applications," *IEEE Commun. Surveys Tuts.*, vol. 11, no. 1, pp. 116–130, 1st Quart., 2009.
[21] W. Qiu, B. Xie, H. Minn, and C.-C. Chong, "Interference-controlled transmission schemes for cognitive radio in frequency-selective time-varying fading channels," *IEEE Trans. Wireless Commun.*, vol. 11, no. 1, pp. 142–153, Jan. 2012.
[22] K. R. Chowdhury and I. F. Akyildiz, "Cognitive wireless mesh networks with dynamic spectrum access," *IEEE J. Sel. Areas Commun.*, vol. 26, no. 1, pp. 168–181, Jan. 2008.
[23] Y. R. Ramadan, Y. Dai, H. Minn, and F. S. Rodrigues, "Spectrum sharing between WiFi and radio astronomy," in *Proc. IEEE Radio Freq. Interference (RFI)*, Oct. 2016, pp. 17–20.
[24] S. S. Bhattacharyya, E. F. Deprettere, R. Leupers, and J. Takala, *Handbook of Signal Processing Systems*. New York, NY, USA: Springer, 2013.
[25] G. Hellbourg, A. P. Chippendale, J. Tuthill, and B. D. Jeffs, "Statistical performance of reference antenna based spatial RFI mitigation for radio astronomy," in *Proc. IEEE Int. Symp. Antennas Propag. USNC/URSI Nat. Radio Sci. Meet.*, Jul. 2015, pp. 1518–1519.
[26] B. D. Jeffs, L. Li, and K. F. Warnick, "Auxiliary antenna-assisted interference mitigation for radio astronomy arrays," *IEEE Trans. Signal Process.*, vol. 53, no. 2, pp. 439–451, Feb. 2005.
[27] A. M. Sardarabadi, A.-J. van der Veen, and A.-J. Boonstra, "Spatial filtering of RF interference in radio astronomy using a reference antenna array," *IEEE Trans. Signal Process.*, vol. 64, no. 2, pp. 432–447, Jan. 2016.
[28] T. L. Wilson, K. Rohlfs, and S. Hüttemeister, *Tools of Radio Astronomy*, vol. 5. New York, NY, USA: Springer, 2009.
[29] A. Colliander *et al.*, "Noise injection radiometer test specifications and requirement," Dept. Elect. Commun. Eng., Helsinki Univ. Technol., Espoo, Finland, Tech. Rep., 2002. [Online]. Avilable: http://urn.fi/urn:nbn:fi:tkk-007772
[30] S. M. Kay, *Fundamentals of Statistical Signal Processing: Estimation Theory*, vol. 1. Englewood Cliffs, NJ, USA: Prentice-Hall, 1993.
[31] P. J. Hall, "Power considerations for the Square Kilometre Array (SKA) radio telescope," in *Proc. IEEE Gen. Assembly Sci. Symp. (URSI)*, Aug. 2011, pp. 1–4.
[32] A. Alekseev. (Jan. 2015). "Basics of low-temperature refrigeration." [Online]. Available: https://arxiv.org/abs/1501.07392
[33] Y. A. Çengel and M. A. Boles, "Thermodynamics: An engineering approach," in *Sea*, vol. 1000. New York, NY, USA: McGraw-Hill, 2015, p. 8862.
[34] L. Grippo and M. Sciandrone, "On the convergence of the block nonlinear Gauss–Seidel method under convex constraints," *Oper. Res. Lett.*, vol. 26, no. 3, pp. 127–136, Apr. 2000.
[35] M. Grant and S. Boyd "CVX: Matlab software for disciplined convex programming, version 2.1," CVX Res. Inc., Tech. Rep., Mar. 2014.

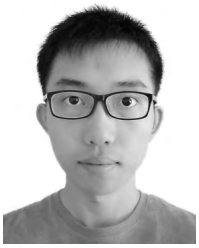

DONG HAN (S'17) received the B.Eng. degree from the University of Electronic Science and Technology of China, Chengdu, China, in 2015, and the M.S. degree from the National University of Singapore, Singapore, in 2016. He is currently pursuing the Ph.D. degree with the Department of Electrical and Computer Engineering, The University of Texas at Dallas, Richardson, TX, USA. He was a Graduate Research Assistant with the Department of Electrical and Computer Engineering, The University of Texas at Dallas. His research interests include wireless communications and signal processing.

HLAING MINN (S'99–M'01–SM'07–F'16) received the B.E. degree in electrical engineering (electronics) from the Yangon Institute of Technology, Yangon, Myanmar, in 1995, the M.Eng. degree in telecommunications from the Asian Institute of Technology, Pathumthani, Thailand, in 1997, and the Ph.D. degree in electrical engineering from the University of Victoria, Victoria, BC, Canada, in 2001. In 2002, he was a Post-Doctoral Fellow with the University of Victoria. He has been with The University of Texas at Dallas since 2002 and is currently a Full Professor. His research interests include wireless communications, signal processing, signal design, dynamic spectrum access and sharing, and next-generation wireless technologies.

Dr. Minn serves as an Editor-at-Large since 2016 and served as an Editor from 2005 to 2016 for the IEEE TRANSACTIONS ON COMMUNICATIONS. He served as a Technical Program Co-Chair for the Wireless Communications Symposium of the IEEE GLOBECOM 2014 and the Wireless Access Track of the IEEE VTC, Fall 2009, as well as a Technical Program Committee Member for several IEEE conferences.